



Published in final edited form as:

Angew Chem Int Ed Engl. 2020 July 13; 59(29): 12154–12161. doi:10.1002/anie.202004449.

Sterically Shielded Heptamethine Cyanine Dyes for Bioconjugation and High Performance Near-Infrared Fluorescence Imaging

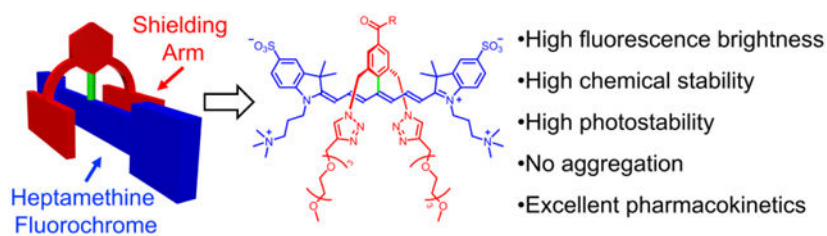
Dong-Hao Li, Cynthia L. Schreiber, Bradley D. Smith*

Department of Chemistry and Biochemistry, University of Notre Dame, 251 Nieuwland Science Hall, University of Notre Dame, Notre Dame, IN 46556, USA

Abstract

The near-infrared window of fluorescent heptamethine cyanine dyes greatly facilitates biological imaging because there is deep penetration of the light and negligible background fluorescence. But dye instability, aggregation, and poor pharmacokinetics are current drawbacks that limit performance and the scope of possible applications. All these limitations are simultaneously overcome with a new molecular design strategy that produces a charge balanced and sterically shielded fluorochrome. The key design feature is a meso-Aryl group that simultaneously projects two shielding arms directly over each face of a linear heptamethine polyene. Cell and mouse imaging experiments compared a shielded heptamethine cyanine dye (and several peptide and antibody bioconjugates) to benchmark heptamethine dyes and found that the shielded systems possess an unsurpassed combination of photophysical, physicochemical and biodistribution properties that greatly enhance bioimaging performance.

Graphical Abstract



Just like a superhero, an ultrastable shielded heptamethine cyanine dye uses its two strong arms to ward off self-aggregation and non-specific biological interactions. Yet the arms are short enough to allow dye-labeled bioconjugates to selectively target cell receptors for high-contrast and photon-intense microscopy or tumor imaging in living subjects.

Keywords

antibodies; cyanines; dyes/pigments; fluorescent probes; imaging agents

* smith.115@nd.edu.

Supporting information for this article is given via a link at the end of the document.

Introduction

Fluorescent heptamethine cyanine dyes (known traditionally and commercially as Cy7) have absorption peaks in the near-infrared (NIR) range of 740–840 nm, a favorable wavelength region for in vivo imaging because there is deep penetration of the light through thick biological samples, along with high image contrast due to decreased light scattering and negligible background signal.^[1] Heptamethine cyanine dyes are often attached to synthetic or biological molecules to create targeted fluorescent conjugates for diagnostics, microscopy, or in vivo imaging of living subjects, and these frontier technologies are expanding rapidly.^[2] The potential value of heptamethine cyanine dyes has increased tremendously in recent years with the realization that the tail of their emission bands extend into the range of 1000–1700 nm which is often called the NIR II region.^[3] This is an important discovery with significant practical implications because in vivo imaging in the NIR II region produces brighter and sharper fluorescence images.

By definition, heptamethine cyanine dyes have extended hydrophobic (and polarizable) surface areas and a small polyene HOMO-LUMO band gap, so dye instability, self-aggregation, and poor pharmacokinetics are common technical drawbacks that severely limit the scope of current applications. Shown in Scheme 1 are leading choices of heptamethine cyanine dyes for fabrication of preclinical and clinical fluorescent NIR molecular probes.^[2b] The archetype heptamethine dye is Indocyanine Green (**ICG**), the only NIR dye with absorption/emission > 700 nm that is approved for use in humans. Although used extensively, it is known for its modest stability and mediocre fluorescent properties, and also the absence of a single reactive site for easy bioconjugation.^[4] A notable advance in heptamethine cyanine chemistry was the development of conjugatable structures with a central cyclohexyl ring.^[5] A benchmark example is polyanionic IRDye CW800® (**CW800**), a commercially available heptamethine indocyanine dye that has been developed into several fluorescent NIR molecular probes that are currently under clinical evaluation for enhanced intraoperative imaging.^[2a,2b] While molecular probes based on **CW800** have undoubted value in biomedical imaging, there are three constraining performance limitations. One is undesired, non-specific interaction of the polyanionic fluorochrome (or its conjugate) with off-target proteins, cell membranes, or skin, which often produces moderate background signals and non-optimal pharmacokinetic profiles.^[3b,6] A second concern is chemical degradation of **CW800** due to nucleophilic displacement of the meso-OAryl group by biological amines or thiols during synthesis, storage, or the course of the imaging experiment.^[7] A third concern is susceptibility to photobleaching due to high reactivity of the electron rich heptamethine polyene with electrophilic singlet oxygen.^[4b,8]

For the last 15 years, international community efforts to solve these three heptamethine cyanine performance problems (non-optimal pharmacokinetics, chemical and photochemical instability) have resulted in two noteworthy structural modifications. In vivo pharmacokinetic profiles have been improved by creating geometrically, charge balanced dye structures (often called zwitterionic) such as **ZW800-1** which minimizes binding to serum proteins and membrane surfaces, promotes exclusive renal clearance, and produces an ultralow imaging background and high Tumor-to-Background ratio.^[6c,9] The second structural improvement is to replace the dye's labile meso C-OAryl bond with a more stable

covalent linkage. A recent advance developed by Schnermann and coworkers employed a more robust meso C-OAlkyl bond,^[6c,8a] and one example of this fluorochrome is **UL766** which exhibits excellent chemical stability and very favorable pharmacokinetics due to its charge balanced structure.^[10] However, the heptamethine polyene within **UL766** (and its close structural analogues) is quite electron rich which means relatively high fluorochrome reactivity with singlet oxygen, and thus susceptibility to photobleaching.^[8a] Another way to replace the reactive meso C-OAryl bond in **ZW800-1** is to employ a much more stable C-C linkage as exemplified by **756z** with its meso-Aryl substituent.^[11] However, the rigid hydrophobic core of charge balanced **756z** (and its close structural analogues) promotes low water solubility and extensive dye self-aggregation which limits practicality.^[11a,11b,12] Self-aggregation of NHS ester versions of **756z** is especially problematic during a protein conjugation reaction because it drives attachment of multiple self-aggregated dyes at proximal lysine positions on the protein surface leading to partially quenched (less fluorescent) protein-dye conjugates.^[12a,13]

Here we present a new and versatile molecular design strategy that simultaneously overcomes all of the heptamethine performance limitations described above. We have invented a new class of cyanine dyes that we call sterically shielded heptamethine cyanine dyes. The molecular design is based on the underappreciated fact that a cyanine dye with a meso-Aryl substituent adopts a low-energy conformation with the plane of the aryl ring strongly rotated out the plane of the polyene.^[14] Adopting this molecular conformation alleviates steric crowding between the meso-Aryl ortho hydrogens and the proximal β hydrogens on the heptamethine chain (Scheme 2). Synthetically, we exploit this structural feature by designing a new three-dimensional architecture that simultaneously projects two shielding arms directly over each face of the polyene. These shielding arms do not greatly increase the molecular weight, but they block undesired biological interactions and enhance photostability. The literature includes a scattering of studies that report self-shielded dyes, but the strategy has not been applied to conjugatable cyanine dyes which are, by far, the most important for NIR fluorescence imaging.^[15] To demonstrate the substantial advantages gained by exploiting this approach, we have prepared a new shielded and charge balanced heptamethine cyanine dye called **s775z** along with two bioconjugates (Scheme 1). We have compared the chemical, photophysical and pharmacokinetic properties of these three fluorescent compounds with an analogous set of compounds that are based on the unshielded analogue **756z** and we find major improvements in several different NIR dye properties that lead to broadly enhanced bioimaging performance.

Results and Discussion

Design and Synthesis

For comparative studies, we synthesized the benchmark heptamethine dye **UL766**^[10] and purchased **ICG**. A more transformational synthetic achievement was to prepare the shielded heptamethine **s775z** and control unshielded analogue **756z**, along with two bioconjugates of each dye. The common structural elements in **s775z** and **756z** include a heptamethine indocyanine fluorochrome and a geometric balanced periphery of cationic and anionic residues. There are two crucial structural differences; the presence of the two shielding arms

in **s775z** as discussed in the introduction section, and the presence of the central cyclohexyl ring in **756z**. While the central cyclohexyl ring bolsters molecular rigidity, which is often considered a favorable structural attribute for fluorescent dyes,^[5a,9c] we reasoned that the rigidity combined with increased hydrophobicity was a factor promoting dye self-aggregation.^[11a,11b,12,16] Literature examples of linear heptamethine polyenes that have a meso-positioned substituent but no central cyclohexyl ring are rare and historically hard to make.^[17] The synthetic advance that allowed us to prepare linear and meso-functionalized **s775z** was the newly reported methodology of Štacková and coworkers that involves ring opening of Zincke salts.^[18] The significant advantage gained by employing this innovative synthetic strategy is that the C-C link to the center of the heptamethine polyene is formed before the complete polyene is created and thus the C-C coupling reaction does not encounter high steric hindrance. The key synthetic intermediate **1** was prepared in five steps and then converted quantitatively into **2** by conducting a copper catalyzed alkyne azide cycloaddition (CuAAC) reaction that attached two triethyleneglycol chains (Scheme 3). The next step was a Zincke reaction; a two-step process that first formed a pyridinium salt, **3**, and then reacted it with two molar equivalents of charge balanced indolenium **4**^[9e] to give the *t*-butyl protected heptamethine dye which was converted into shielded **s775z**.

Molecular Structure of s775z

The energy minimized molecular model of **s775z** in Scheme 2 shows how the two shielding arms, with triethyleneglycol chains, project over both faces of the heptamethine polyene that is an all-trans conformation.^[4a] The model is consistent with literature X-ray crystal structures showing the meso-Aryl ring strongly rotated out of the plane of the polyene.^[14,19] Close inspection of the ¹H NMR spectra for **s775z** (Figure S3) in water reveals the heptamethine proton coupling constants (³J_{HH}) to all be 13.5 Hz indicating a polyene chain with an all-trans conformation.^[20] In addition, ¹H-¹H NOE experiments (Figure S4) identified cross relaxation between indolenine gem-dimethyl protons and polyene protons, as well as shielding chain protons, all consistent with an all-trans polyene.^[21] Finally, the chemical shifts for the heptamethine β-protons and indolenine gem-dimethyl groups in **756z** and **s775z** are substantially upfield of the analogous peaks in related heptamethine structures that do not have a meso-Aryl substituent (Figure S2), reflecting strong magnetic shielding of these diagnostic protons by the face of the rotated meso-Aryl ring.

Spectral Properties and Stability

As shown in Tables 1, S1 and S2, the fluorescence brightness of shielded **s775z** and benchmark **UL766** were listed within experimental error. Importantly, the excitation/emission wavelengths of **s775z** (ex: 775 nm, em: 794, in PBS) closely match the typical default settings of commercial closed box and open field imaging stations, which means minimal refinement of machine configuration is needed for future utilization of molecular probes that are based on **s775z**.^[22]

Aqueous samples of **s775z** can be stored indefinitely at 4°C, and samples of **s775z** in 100% fetal bovine serum (FBS) do not change at 37 °C over 24 hours (Figure S13a) which is in contrast to the known degradation of **CW800** and **ZW800-1** under very similar conditions.^[10,12]

High photostability is also a highly desired, but an elusive heptamethine cyanine dye property.^[4a,24] Photobleaching of a heptamethine cyanine dye is primarily caused by a bimolecular reaction of the heptamethine polyene with photogenerated singlet oxygen.^[4b,8a-c] The predominant reaction pathway forms a strained dioxetane intermediate followed by a fragmentation cascade. A possible second minor pathway is electron transfer from the polyene to singlet oxygen leading to a dimerized dye structure.^[20]

Shown in Figure 1 are the results of two separate photostability studies. The first study irradiated four different cuvettes, each containing a solution of dye in PBS, with a Xenon lamp (filtered to allow wavelengths > 620 nm) and monitored for a decrease in the dye's absorption maxima band (Figure 1a, see Figures S15–S18 for the entire set of spectral plots and Table S3 for quantification). The order of photostabilities was observed to be **s775z** > **756z** > **UL766** > **ICG**. An additional competitive experiment irradiated a single solution containing a mixture of **s775z** and **UL766** which ensured that both dyes were exposed to the same number of photons and photogenerated singlet oxygen. Analysis of the solution mixture after irradiation revealed slight decomposition of the **s775z** but complete loss of all **UL766** (Figure S19).

A second, independent photostability study confirmed the difference between **s775z** and **UL766** under milder irradiation conditions that more closely resembled an in vivo imaging experiment or clinical intraoperative imaging procedure. Imaging phantoms were created by immobilizing stable drops of **s775z** or **UL766** (100 μ L, 10 μ M in PBS buffer, pH 7.4) on a black non-reflective sheet. The phantoms were placed inside a commercial in vivo imaging station and continuously exposed to the station's 745 nm LED. The data in Figure 1b shows the change in mean pixel intensity (MPI) for the phantom images. After 60 min of constant irradiation, the images of phantoms containing **UL766** had decreased to 58 ± 2 % of initial intensity; whereas, the images of phantoms containing **s775z** had only decreased to 77 ± 2 % of initial intensity.

These heptamethine photostability trends suggest that the meso-Aryl group in **s775z** with its two shielding arms induces three synergistic effects that inhibit bimolecular reaction of its heptamethine polyene with electrophilic singlet oxygen: (a) the meso-Aryl group within **s775z** electronically deactivates polyene reactivity (lowers the HOMO energy) compared to **UL766** which has an electron donating meso-OAlkyl group, (b) the steric bulk of the meso-Aryl group in **s775z** destabilizes any putative dioxetane intermediate formed by oxygen/polyene cycloaddition, and (c) the two shielding arms in **s775z** sterically inhibit singlet oxygen attack at the polyene, compared to unshielded **756z**, providing more opportunity for the short-lived singlet oxygen to relax by another physical pathway.^[15e]

Aggregation of Dyes and Bioconjugates

The solubility of **s775z** in water is remarkably high at >100 mM and a 1 mM stock solution of **s775z** in water was found to be unchanged after one month storage at 4 °C. In contrast, a freshly prepared 1 mM stock solution of unshielded **756z** in water forms a precipitate after 24 hr, and the insoluble material cannot be redissolved after sonication (Figure S1). The difference in water solubility between **s775z** and **756z** correlates with the propensities to

form self-aggregates. Self-aggregation of heptamethine cyanine dyes is readily indicated by conversion of monomer absorption bands into aggregate bands, in this case blue-shifted H-aggregates.^[13b,13c] As shown by the absorption spectra in Figures 2a and S7–S10, the control dye **756z** exists largely as non-fluorescent H-aggregates (see excitation spectra in Figure S11), whereas the shielded dye **s775z** is in a fluorescent monomeric state. A series of dye/protein association studies (Figures S10 and S14) found that charge balanced **756z** and **s775z** have similar weak affinities for bovine serum albumin (BSA) with K_a values of $1.6 \times 10^4 \text{ M}^{-1}$ and $1.3 \times 10^4 \text{ M}^{-1}$, respectively, which is about 40 times lower than the K_a for BSA association with **ICG**.^[13b,25]

Standard amide bond conjugation chemistry was used to react the NHS ester of **756z** or **s775z** with a free amine on the cyclic peptide targeting unit, cRGDFK, and create the homologous fluorescent peptide probes **756z-RGD** and **s775z-RGD**, respectively (Scheme 1). The absorption spectra in Figure 2b and Figure S12 show that the unshielded probe **756z-RGD** exists as a concentration-dependent mixture of fluorescent monomer and non-fluorescent H-aggregate (see excitation spectrum in Figure S11), whereas the shielded probe **s775z-RGD** is a fluorescent monomer in water even at the highest concentration tested (10 μM).

Amide bond formation was also used to attach multiple copies of either **756z** or **s775z** to an antibody. Two sets of antibody conjugates were each prepared by reacting goat Immunoglobulin G (IgG) with dye NHS ester followed by size exclusion purification to remove any unreacted dye (see Figures S20–S22 for gel electrophoresis proof-of-purity). Purified samples of **756z-IgG** (degree of labeling (DOL) = 2.1) and **s775z-IgG** (DOL = 2.3) were found to be stable over 7 days when stored at 4 °C in PBS buffer (Figure S25), unlike antibody conjugates of **ZW800-1** which have been reported to partially degrade over 24 hours.^[12b] The absorption spectrum of control antibody conjugate **756z-IgG** (Figure 3a) shows a blue-shifted H-aggregate peak at 680 nm corresponding to close stacking of the appended fluorochromes because they are attached to the antibody at proximal positions (see Scheme S1 for a schematic picture).^[13] A patch of stacked appended fluorescent dyes on an antibody surface is problematic for several reasons, including: (a) the stacked dyes can disrupt antibody folding or structural dynamics and thus antibody function; (b) the H-aggregate peak is non-fluorescent which weakens utility of the antibody conjugate for high sensitivity fluorescence imaging or diagnostics; (c) a patch of stacked appended dyes can become a hydrophobic hot spot on the antibody surface and promote undesired antibody aggregation or association with biological interfaces. This latter point became apparent when we prepared versions of control **756z-IgG** with DOL > 2.1; absorption spectra for these samples indicated extensive light scattering (Figure S24) due to intermolecular aggregation of the antibody conjugate. In stark contrast, the absorption spectrum of an analogous antibody conjugate, **s775z-IgG**, did not exhibit a stacked fluorochrome peak (Figure 3a). Shown in Figure 3b is a plot of relative fluorescence intensity for different polyacrylamide gel bands comprised of **s775z-IgG** with increasing DOL. The plot reveals an inverse exponential dependence of relative fluorescence on DOL, up to the highest DOL tested which was 10.7. Even at this unusually high DOL, there was no stacked fluorochrome peak in the conjugate's absorption spectrum (Figure S23), indicating that the 10.7 (on average)

copies of **s775z** covalently appended to the surface of the IgG were not spatially close enough for strong Coulombic coupling of dye excitons.^[26] The fact that fluorescence intensity for **s775z-IgG** continually increases with DOL, without reaching a maximum value, is unusual for a protein labeled with a cyanine dye, especially a heptamethine cyanine.^[12a,27] This finding has important practical implications because it suggests that bright, densely labeled **s775z**-antibodies can be used at very low doses for diagnostics or imaging applications. This is crucial in the field of fluorescence guided surgery where the procedural and practical benefits of conducting clinical trials under microdosing regimes are well recognized,^[28] but to date very few microdose trials have been attempted with fluorescent antibodies because they are not sufficiently bright.^[2a,29]

Biological Imaging Studies

The overall goal of the biological imaging studies was to determine if the heptamethine steric shielding effect promoted high performance NIR fluorescence imaging. More specifically, we needed to prove that the length of the shielding triethyleneglycol chains in **s775z** was long enough to block non-specific interactions with membrane surfaces, serum proteins, and the extracellular matrix. Yet the shielding arms had to be short enough to permit strong association of dye-labeled bioconjugates with specific cell receptors and also allow rapid renal excretion of any unbound probe.^[30]

The hypothesis of low non-specific binding was first tested by measuring the cell uptake, cell toxicity, and mouse biodistribution of **s775z**. Cell microscopy experiments showed negligible cell uptake of **s775z**, and there was no significant drop in cell viability after 24 hours of dye incubation at the low micromolar concentrations commonly used for biological imaging (Figure S26). Mouse biodistribution studies injected two separate cohorts of normal mice with a 10 nmol dose of **ICG** or **s775z**, followed by whole body imaging over time (all mouse experiments used protocols that were approved by the university's Institutional Animal Care and Use Committee). After 2 hours the mice were sacrificed and the abdominal cavity of each animal was exposed and imaged. The live mouse images (Figure S28a) showed that both dyes were quickly cleared from the mouse bloodstream. But as revealed by the representative NIR images of exposed abdomen in Figure 4a and the associated biodistribution graph (Figure S28b), the blood clearance pathways were very different. As expected, virtually all of the **ICG** remained within the animals, where it accumulated in the intestines and liver. In contrast, most of the **s775z** had undergone near-exclusive renal clearance after 2 hours, with only weak NIR fluorescence remaining in the urine-containing bladder and kidneys.

The next step was to prove that the two shielding triethyleneglycol chains in **s775z** did not prevent a targeted version of the dye from binding to cancer cell-surface receptors. This was done by first studying the cell targeting properties of the peptide conjugates, **s775z-RGD** and **756z-RGD**. These two conjugates include the cyclic peptide sequence cRGDfK that is well-known to have nanomolar affinity for cell-surface integrin receptors, more specifically the receptor sub-types $\alpha_v\beta_3$ and $\alpha_v\beta_5$.^[31] The ubiquity of RGD-based molecular probes makes cRGDfK a sensible choice of targeting unit for comparative studies of biological imaging performance.^[2a,2b] We focused on A549 cancer cells (human lung adenocarcinoma)

which is a cell line that overexpresses integrin $\alpha_v\beta_5$ receptors and selectively internalizes fluorescent cRGDfK conjugates.^[31,32] A comparative set of fluorescence microscopy experiments incubated separate samples of A549 cells with each fluorescent compound (**s775z-RGD**, **756z-RGD**, **s775z**, or **756z**) and observed much higher cell uptake of two cRGDfK targeted probes compared to their untargeted counterparts (Figure S27). Moreover, cell uptake of the shielded **s775z-RGD** was higher than cell uptake of the unshielded and self-aggregated **756z-RGD**. In both cases, the cell uptake of targeted probe was successfully blocked by pre-incubating the cells with an excess amount of the optically transparent targeting peptide cRGDfK (Figure 4b), strongly indicating that cell uptake was caused by integrin-selective binding and subsequent endocytosis.

The high level of A549 cell uptake by cancer targeted **s775z-RGD** prompted us to conduct in vivo imaging studies using a subcutaneous mouse tumor model. Nude mice (N=8) bearing a subcutaneous tumor (A549 cells) in the right rear flank were randomly divided into two cohorts and given a retro-orbital injection of either **s775z** or **s775z-RGD** (10 nmol).^[33] Each mouse was imaged periodically over 3 hours (Figure 4c and S29) and the change in tumor fluorescence MPI and Tumor-to-Background ratio was plotted (Figure 4d and S30). The live animal images were consistent with the standard pharmacokinetic model for tumor partitioning of small untargeted and targeted probes.^[25,34] The mice dosed with **s775z** showed transient uptake into the subcutaneous tumor followed by washout of the untargeted dye. In contrast, the images of mice dosed with the targeted **s775z-RGD** showed much slower washout from the tumor leading to a significantly higher Tumor-to-Background ratio at the 2 hour and 3 hour time points (Figures 4d and S29–S30). This difference in tumor imaging capability reflects the high affinity of the targeted **s775z-RGD** probe for the overexpressed integrin receptors on the surface of the cancer cells and endothelial cells that line the tumor vasculature.^[32] After the 3 hour time point, the mice were sacrificed, and a mock surgery was performed on the mouse cohort dosed with **s775z-RGD** (Figure S31). Subsequently, all tumors and major organs were removed and the amount of dye in the different tissues was quantified by measuring the fluorescence MPI. Shown in Figure 4e is a plot of MPI for excised tumors, normalized to thigh muscle, and also a pair of representative NIR fluorescence images of the excised tumors. The complete set of tumor NIR fluorescence images is provided in Figure S32 and a plot of normalized MPI for all excised tissues is shown in Figure S33. The normalized tumor MPI for mice dosed with cancer targeted **s775z-RGD** (14.4 ± 3.0) was much higher than the value for mice dosed with untargeted **s775z** (2.6 ± 0.5), and reflects a combination of high affinity for the overexpressed integrin receptors in the tumor tissue and very low affinity for background muscle tissue.^[9d,33] From the perspective of fluorescence guided cancer surgery, **s775z-RGD** achieved the highly desirable combination of rapid, near-exclusive renal clearance from the bloodstream, very high Tumor-to-Background ratio, and ultralow retention in background tissue.^[2a,2b] Thus, **s775z-RGD** has high potential for passage towards clinical translation.

Conclusion

For about thirty years, chemical research on heptamethine cyanine dyes has focused on flat molecules with a polar periphery. This study validates a new three-dimensional structural strategy that simultaneously projects two shielding arms directly over each face of the polyene. Compared to the benchmark heptamethine cyanine dyes listed in Scheme 1, shielded **s775z** and its bioconjugates exhibit an unsurpassed combination of photophysical, physiochemical and biodistribution properties that greatly enhance bioimaging performance. Shielded **s775z** has a C-Aryl group at the meso position of a heptamethine polyene which makes the fluorochrome chemically more stable than the popular heptamethine cyanines **CW800** or **ZW800-1** which each have a more labile meso C-OAryl linkage.^[12] A large set of comparative NIR fluorescence studies compared **s775z** to unshielded control dye **756z** and found that shielding prevents dye self-aggregation and non-specific biological interactions. Importantly, the shielding arms do not prevent high affinity targeting of bioconjugates to cell surface receptors, or renal clearance from the blood stream. Notably, the integrin targeted probe **s775z-RGD** permitted high contrast cancer cell microscopy and mouse tumor imaging, with the latter producing a very high Tumor-to-Background ratio and ultralow retention in background tissue. Additional bioconjugation studies showed that multiple copies of shielded **s775z** can be attached to an antibody to produce a densely labeled conjugate without any stacking of appended fluorochromes. Next generation versions of densely labeled **s775z**-antibodies can likely be used as very bright, fluorescent probes for deployment at microdoses in various diagnostics or clinical imaging procedures. Furthermore, shielded **s775z** exhibits much better photostability than the benchmark heptamethine cyanines **CW800**, **ZW800-1**, or **UL766** whose polyenes are electronically activated to react with photogenerated singlet oxygen. The remarkably high photostability of **s775z** makes it very attractive for incorporation into modern photon-intensive microscopy experiments such as single molecule tracking or super resolution imaging, as well as emerging clinical procedures, such as fluorescence guided surgery, which require long periods of sustained light exposure.^[4a] The synthetic modularity that underlies the structure of **s775z** enables easy customization of bioimaging performance by modifying the two shielding arms to rationally fine-tune pharmacokinetics,^[30,35] or the polyene structure to enhance photophysical properties.^[36]

Supplementary Material

Refer to Web version on PubMed Central for supplementary material.

Acknowledgements

We are grateful for funding support from the US NIH (R01GM059078, R35GM136212 and T32GM075762) and a Berry Family Foundation fellowship from the University of Notre Dame.

References

- [1]. a)Sun W, Guo S, Hu C, Fan J, Peng X, Chem. Rev 2016, 116, 7768–7817; [PubMed: 27314280]
b)Shi C, Wu JB, Pan D, J. Biomed. Opt 2016, 21, 050901.

- [2]. a)Hernot S, Manen LV, Debie P, Sven J, Mieog D, Vahrmeijer AL, *Lancet Oncol.* 2019, 20, e354–e367; [PubMed: 31267970] b)Debie P, Hernot S, *Front. Pharmacol* 2019, 10, 510; [PubMed: 31139085] c)Levitus M, Ranjit S, *Q. Rev. Biophys* 2011, 44, 123–151. [PubMed: 21108866]
- [3]. a)Zhu S, Yung BC, Chandra S, Niu G, Antaris AL, Chen X, *Theranostics* 2018, 8, 4141–4151; [PubMed: 30128042] b)Zhu S, Hu Z, Tian R, Yung BC, Yang Q, Zhao S, Kiesewetter DO, Niu G, Sun H, Antaris AL, Chen X, *Adv. Mater* 2018, 30, 1802546.
- [4]. a)Gorka AP, Nani RR, Schnermann MJ, *Acc. Chem. Res* 2018, 51, 3226–3235; [PubMed: 30418020] b)Gorka AP, Nani RR, Schnermann MJ, *Org. Biomol. Chem* 2015, 13, 7584–7598. [PubMed: 26052876]
- [5]. a)Ma X, Laramie M, Henary M, *Bioorg. Med. Chem. Lett* 2018, 28, 509–514; [PubMed: 29249562] b)Strekowski L, Lipowska M, Patonay G, *J. Org. Chem* 1992, 57, 4578–4580.
- [6]. a)Debie P, van Quathem J, Hansen I, Bala G, Massa S, Devoogdt N, Xavier C, Hernot S, *Mol. Pharm* 2017, 14, 1145–1153; [PubMed: 28245129] b)Cilliers C, Nessler I, Christodolu N, Thurber GM, *Mol. Pharm* 2017, 14, 1623–1633; [PubMed: 28294622] c)Sato K, Gorka AP, Nagaya T, Michie MS, Nani RR, Nakamura Y, Coble VL, Vasalatiy OV, Swenson RE, Choyke PL, Schnermann MJ, Kobayashi H, *Bioconjug. Chem* 2016, 27, 404–413; [PubMed: 26444497] d)Owens EA, Henary M, Fakhri G. El, Choi HS, *Acc. Chem. Res* 2016, 49, 1731–1740; [PubMed: 27564418] e)Bunschoten A, Welling MM, *Bioconjug. Chem* 2016, 27, 1253–1258; [PubMed: 27074375] f)Yu M, Liu J, Ning X, Zheng J, *Angew. Chem. Int. Ed* 2015, 54, 15434–15438; *Angew. Chem.* 2015, 127, 15654–15658;g)Sato K, Paik CH, Schnermann MJ, Gorka AP, Nagaya T, Nakamura Y, Harada T, Shaum JB, Kim I, Kobayashi H, Nani RR, Choyke PL, *Mol. Pharm* 2015, 12, 3303–3311. [PubMed: 26261913]
- [7]. a)Lim SY, Hong KH, Kim DI, Kwon H, Kim HJ, *J. Am. Chem. Soc* 2014, 136, 7018–7025; [PubMed: 24754635] b)Zaheer A, Wheat TE, Frangioni JV, *Mol. Imaging* 2002, 1, 354–364. [PubMed: 12926231]
- [8]. a)Luciano MP, Crooke SN, Nourian S, Dingle I, Nani RR, Kline G, Patel NL, Robinson CM, Diflippantonio S, Kalen JD, Finn MG, Schnermann MJ, *ACS Chem. Biol* 2019, 14, 934–940; [PubMed: 31030512] b)Nani RR, Kelley JA, Ivanic J, Schnermann MJ, *Chem. Sci* 2015, 6, 6556–6563; [PubMed: 26508998] c)Samanta A, Vendrell M, Das R, Chang Y-T, *Chem. Commun* 2010, 46, 7406–7408;d)Mellanby RJ, Scott JI, Mair I, Fernandez A, Saul L, Arlt J, Moral M, Vendrell M, *Chem. Sci* 2018, 9, 7261–7270. [PubMed: 30288247]
- [9]. a)Yang Z, Usama SM, Li F, Burgess K, Li Z, *Med. Chem. Comm* 2018, 31, 1754–1760;b)Hyun H, Henary M, Gao T, Narayana L, Owens EA, Lee JH, Park G, Wada H, Ashitate Y, Frangioni JV, Choi HS, *Mol. Imaging Biol* 2016, 52–61; [PubMed: 26084246] c)Choi HS, Narayana L, Henary M, Njiojob CN, Owens EA, Hyun, J. *Med. Chem* 2015, 58, 2845–2854; [PubMed: 25711712] d)Choi HS, Gibbs SL, Lee JH, Kim SH, Ashitate Y, Liu F, Hyun H, Park G, Xie Y, Bae S, Henary M, Frangioni JV, *Nat. Biotechnol* 2013, 31, 148–153; [PubMed: 23292608] e)Choi HS, Nasr K, Alyabyev S, Feith D, Lee JH, Kim SH, Ashitate Y, Hyun H, Patonay G, Streckowski L, Henary M, Frangioni JV, *Angew. Chem. Int. Ed* 2011, 50, 6258–6263; *Angew. Chem.* 2011, 123, 6382–6387.
- [10]. Cha J, Nani RR, Luciano MP, Kline G, Broch A, Kim K, Namgoong J.-m., Kulkarni RA, Meier JL, Kim P, Schnermann MJ, *Bioorg. Med. Chem. Lett* 2018, 28, 2741–2745. [PubMed: 29510880]
- [11]. a)Su D, Teoh CL, Samanta A, Kang NY, Park SJ, Chang YT, *Chem. Commun* 2015, 51, 3989–3992;b)Wu Z, Shao P, Zhang S, Bai M, *J. Biomed. Opt* 2014, 19, 36006; [PubMed: 24604536] c)Lee H, Mason JC, Achilefu S, *J. Org. Chem* 2006, 71, 7862–7865. [PubMed: 16995699]
- [12]. a)van der Wal S, Kuil J, Valentijn ARPM, van Leeuwen FWB, *Dyes Pigm.* 2016, 132, 7–19;b)Hyun H, Owens EA, Narayana L, Wada H, Gravier J, Bao K, Frangioni JV, Choi HS, Henary M, *RSC Adv.* 2014, 4, 58762–58768. [PubMed: 25530846]
- [13]. a)Ji Y, Wang Z, Bao K, Park GK, Kang H, Hu S, McDonald E, Kim MS, Kashiwagi S, Choi HS, *Quant. Imaging Med. Surg* 2019, 9, 1548–1555; [PubMed: 31667140] b)Spa SJ, Hensbergen AW, van der Wal S, Kuil J, van Leeuwen FWB, *Dyes Pigm.* 2018, 152, 19–28;c)Gruber HJ, Hahn CD, Kada G, Riener CK, Harms GS, Ahrer W, Dax TG, Knaus H-GG, *Bioconjug. Chem* 2000, 11, 696–704. [PubMed: 10995214]

- [14]. a)Al-Karmi S, Albu SA, Vito A, Janzen N, Czorny S, Banevicius L, Nanao M, Zubieta J, Capretta A, Valliant JF, Chem. Eur. J 2017, 23, 254–258; [PubMed: 27768812] b)He L, Lin W, Xu Q, Ren M, Wei H, Wang J-Y, Chem. Sci 2015, 6, 4530–4536. [PubMed: 28717473]
- [15]. a)Ji C, Cheng W, Yuan Q, Mullen K, Yin M, Acc. Chem. Res 2019, 52, 2266–2277; [PubMed: 31373482] b)Kühne C, Haag R, Heek T, Urner LH, Pagel K, Huth K, Achazi K, Dermedde J, Chem. Eur. J 2017, 23, 4849–4862; [PubMed: 28128483] c)Zhu S, Yang Q, Antaris AL, Yue J, Ma Z, Wang H, Huang W, Wan H, Wang J, Diao S, Zhang B, Li X, Zhong Y, Yu K, Hong G, Luo J, Liang Y, Dai H, Proc. Natl. Acad. Sci. U.S.A 2017, 114, 962–967; [PubMed: 28096386] d)Wycisk V, Pauli J, Welker P, Justies A, Resch-Genger U, Haag R, Licha K, Bioconjug. Chem 2015, 26, 773–781; [PubMed: 25811535] e)Yau CMS, Pascu SI, Odom SA, Warren JE, Klotz E, Frampton MJ, Williams CC, Coropceanu V, Kuimova MK, Phillips D, Barlow S, Brédas JL, Marder SR, Millar V, Anderson HL, Chem. Commun 2008, 2897–2899.
- [16]. Thavornpradit S, Usama SM, Park GK, Shrestha JP, Nomura S, Baek Y, Choi HS, Burgess K, Theranostics 2019, 9, 2856–2867. [PubMed: 31244928]
- [17]. Arjona-Esteban A, Stolte M, Würthner F, Angew. Chem. Int. Ed 2016, 55, 2470–2473; Angew. Chem. 2016, 128, 2516–2519.
- [18]. Štacková L, Štacko P, Klán P, J. Am. Chem. Soc 2019, 141, 7155–7162. [PubMed: 31017409]
- [19]. The Cambridge Crystallographic Data Centre contains relevant X-ray structures, including: 1404767, 1404768 and 1404769.
- [20]. Rüttger F, Mindt S, Golz C, Alcarazo M, John M, Eur. J. Org. Chem 2019, 2019, 4791–4796.
- [21]. At present, we cannot rule out the possibility that a small fraction of s775z adopts a polyene conformation with one of its methine-methine bonds in a cis orientation (this putative conformational exchange would be rapid on the NMR time scale, see reference 20 for further discussion). This minor structural point does not change any conclusions concerning the practical value of s775z.
- [22]. DSouza AV, Lin H, Henderson ER, Samkoe KS, Pogue BW, J. Biomed. Opt 2016, 21, 080901.
- [23]. a)Hyun H, Bordo MW, Nasr K, Feith D, Lee JH, Kim SH, Ashitate Y, Moffitt LA, Rosenberg M, Henary M, Choi HS, Frangioni JV, Contrast Media Mol. Imaging 2012, 7, 516–524; [PubMed: 22991318] b)Ohnishi S, Lomnes SJ, Laurence RG, Gogbashian A, Mariani G, Frangioni JV, Mol. Imaging 2005, 4, 172–181. [PubMed: 16194449]
- [24]. König SG, Krämer R, Chem. Eur. J 2017, 23, 9306–9312. [PubMed: 28339120]
- [25]. Berezin MY, Guo K, Akers W, Livingston J, Solomon M, Lee H, Liang K, Agee A, Achilefu S, Biochemistry 2011, 50, 2691–2700. [PubMed: 21329363]
- [26]. Szabó Á, Szendi-Szalmáry T, Ujlaky-Nagy L, Rádi I, Vereb G, Szöllősi J, Nagy P, Biophys. J 2018, 114, 688–700. [PubMed: 29414714]
- [27]. Berlier JE, Rothe A, Buller G, Bradford J, Gray DR, Filanoski BJ, Telford WG, Yue S, Liu J, Cheung CY, Chang W, Hirsch JD, Beechem JM, Haugland RP, Haugland RP, J. Histochem. Cytochem 2003, 51, 1699–1712. [PubMed: 14623938]
- [28]. Kleinjan GH, Bunschoten A, Berg NSVD, Eur. J. Nuc. Med. Mol. Imaging 2016, 1857–1867.
- [29]. Lamberts LE, Koch M, Jong JSD, Adams ALL, Kranendonk EG, Scheltinga AGTTV, Jorritsma-Smit A, Linsen MD, Boer ED, Vegt BVD, Nagengast WB, Elias SG, Oliveira S, Witkamp AJ, Wall EVD, Diest PJV, Vries EGED, Clin. Cancer Res 2017, 23, 2730–2742. [PubMed: 28119364]
- [30]. Du B, Jiang X, Huang Y, Li S, Lin JC, Yu M, Zheng J, Bioconjug. Chem 2019, 31, 241–247. [PubMed: 31697893]
- [31]. Shaw SK, Liu W, Gómez-Durán CFA, Schreiber CL, Betancourt-Mendiola M. de L., Zhai C, Roland FM, Padanilam SJ, Smith BD, Chem. Eur. J 2018, 24, 13821–13829. [PubMed: 30022552]
- [32]. Schreiber CL, Zhai C, Dempsey JM, Mcgarraugh HH, Matthews BP, Christmann CR, Smith BD, Bioconjug. Chem 2020, 31, 214–223. [PubMed: 31756298]
- [33]. Handgraaf HJM, Boonstra MC, Prevoo HAJM, Kuil J, Bordo MW, Boogerd LSF, Sibinga Mulder BG, Sier CFM, Vinkenburg-van Slooten ML, Valentijn ARPM, Burggraaf J, van de Velde CJH, Frangioni JV, Vahrmeijer AL, Oncotarget 2017, 8, 21054–21066. [PubMed: 28416744]

- [34]. Tichauer KM, Samkoe KS, Sexton KJ, Hextrum SK, Yang HH, Klubben WS, Gunn JR, Hasan T, Pogue BW, *Mol. Imaging Biol* 2012, 14, 584–592. [PubMed: 22203241]
- [35]. Yazaki PJ, Lwin TM, Minnix M, Li L, Sherman A, Molnar J, Miller A, Frankel P, Chea J, Poku E, Bowles N, Hoffman RM, Shively JE, Bouvet M, *J. Biomed. Opt* 2019, 24, 066012.
- [36]. a) Michie MS, Götz R, Franke C, Bowler M, Kumari N, Magidson V, Levitus M, Loncarek, Sauer M, Schnermann MJ, *J. Am. Chem. Soc* 2017, 139, 12406–12409; [PubMed: 28862842] b) Li B, Lu L, Zhao M, Lei Z, Zhang F, *Angew. Chem. Int. Ed* 2018, 57, 7483–7487; *Angew. Chem.* 2018, 130, 7605–7609.

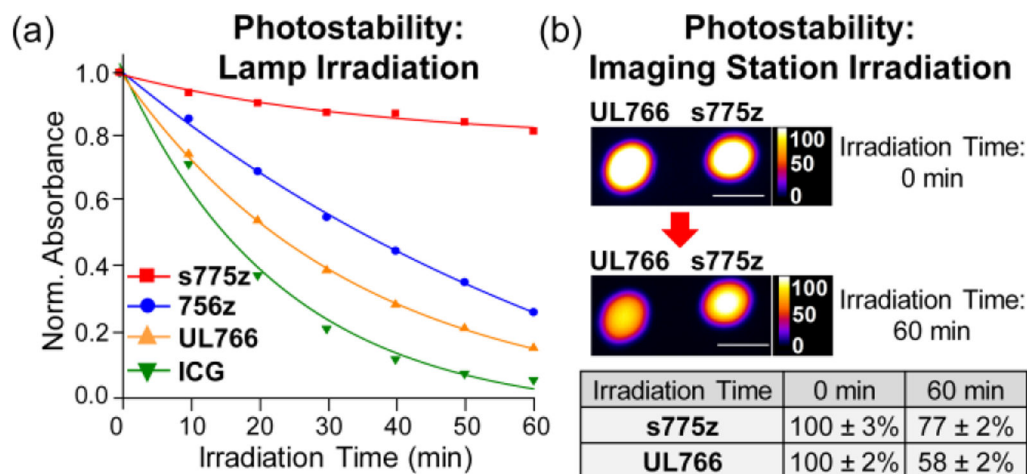


Figure 1.

Two separate photostability studies. (a) Lamp irradiation: Four separate cuvettes, each containing 1 μM dye in PBS buffer, pH 7.4, were irradiated by a 150 W Xenon lamp with a 620 nm long-pass filter. The plot of normalized dye absorbance versus time was fit to a one-phase exponential decay. (b) Imaging station irradiation: Imaging phantoms (immobilized 100 μL drops containing **s775z** or **UL766**, 10 μM in PBS buffer, pH 7.4) were irradiated with an in vivo imaging station's 745 nm LED for a total period of 60 min. The mean pixel intensity (MPI) values for the fluorescence images (ex: 745 nm, em: 850 nm) are listed (N=3 for each phantom). The length scale bar on each NIR fluorescence image is 1 cm.

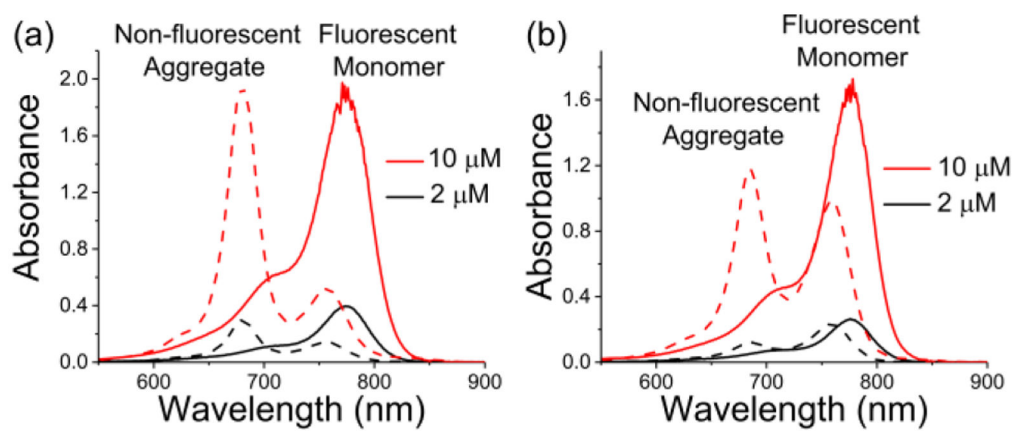


Figure 2. Absorption spectra. (a) *s775z* (solid line) and *756z* (dashed line), (b) *s775z-RGD* (solid line) and *756z-RGD* (dashed line), in water at different concentrations.

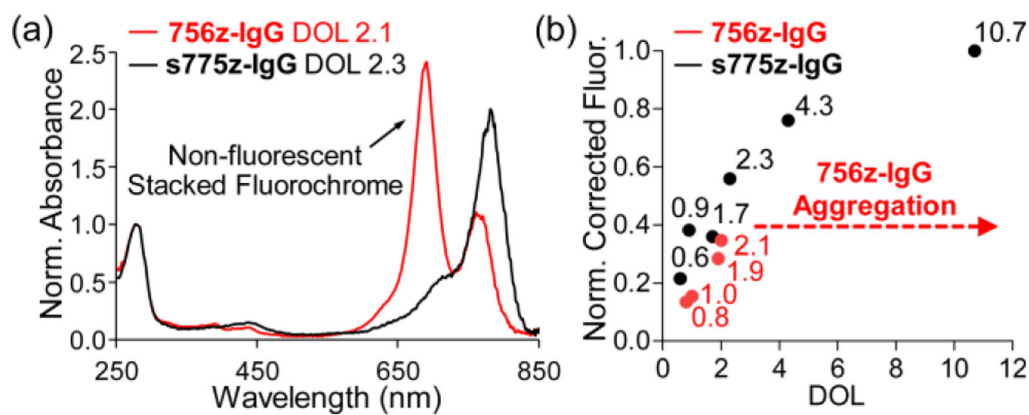
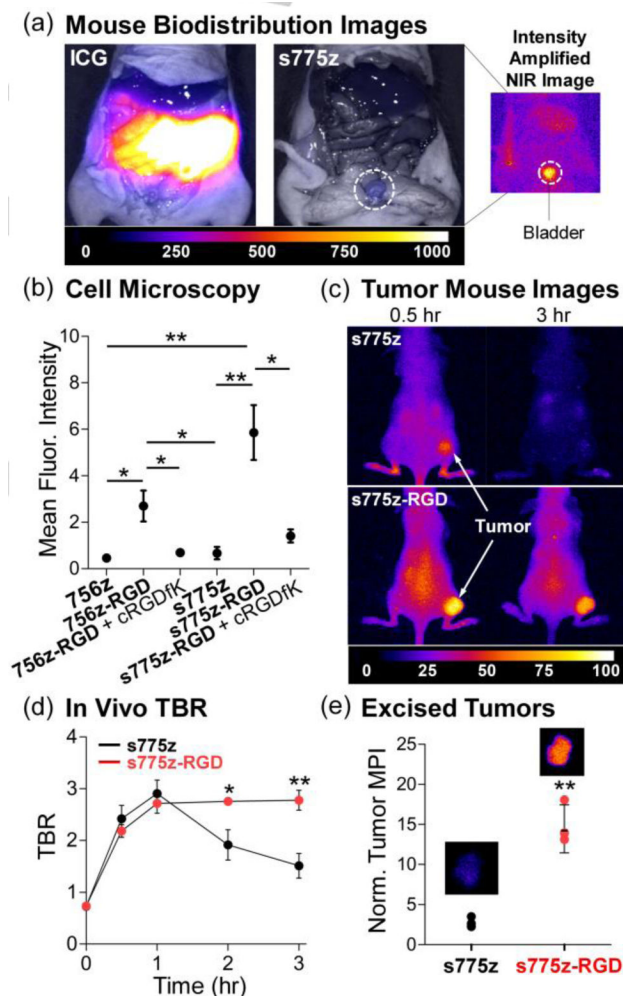
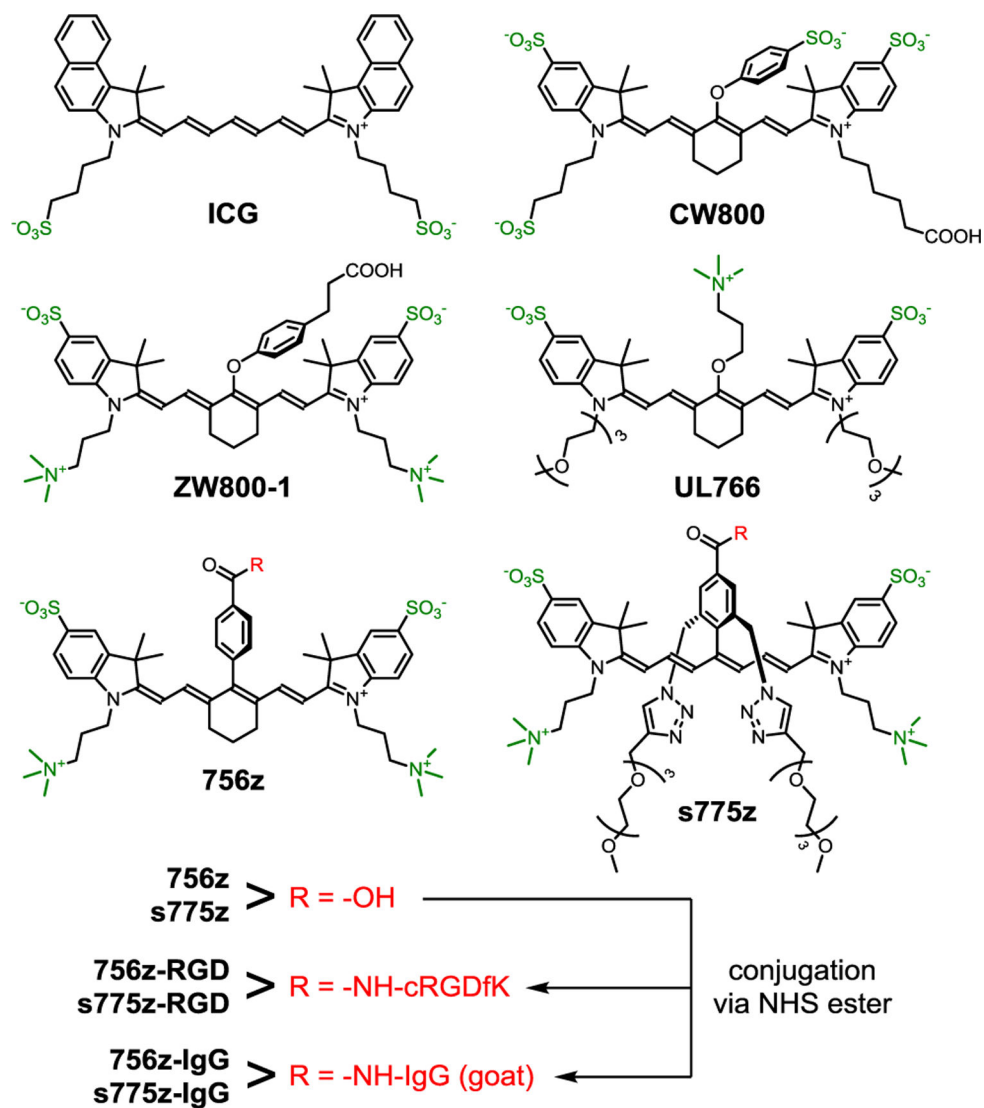


Figure 3.

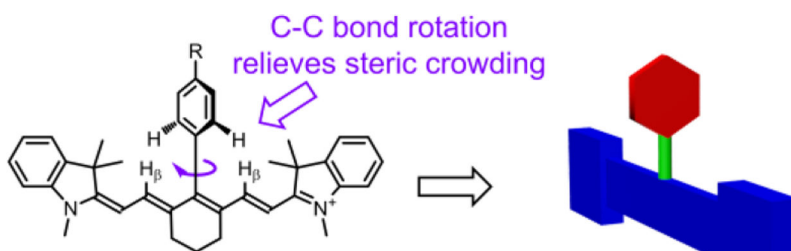
(a) Absorbance spectra (normalized to the absorbance at 280 nm) for samples of **756z-IgG** or **s775z-IgG** with very similar DOL. Only the **756z-IgG** spectrum exhibits a blue-shifted peak corresponding to non-fluorescent stacked fluorochrome. (b) Plot of DOL for **756z-IgG** or **s775z-IgG** versus fluorescence intensity (corrected for protein concentration and normalized relative to **s775z-IgG** DOL 10.7) for different bands of pure **756z-IgG** or **s775z-IgG** on a polyacrylamide gel.

**Figure 4.**

(a) Representative overlaid brightfield and fluorescence images of exposed abdomen of normal mice (no tumor) sacrificed 2 hr after retro-orbital injection of either **ICG** or **s775z** (10 nmol). The fluorescence intensity scale, in arbitrary units, is the same for both overlaid images, whereas the intensity of smaller NIR fluorescence image is amplified. (b) Plot of intracellular mean fluorescence intensities as a measure of NIR dye cell uptake. Integrin positive A549 cells were treated for 1 hr with 10 μ M of NIR probe. The blocking experiments added 100 μ M of free cRGDfK prior to the incubation with RGD probes. (c) Representative whole-body NIR fluorescence images of living mice bearing a subcutaneous A549 tumor at 0.5 and 3 hr after retro-orbital injection of either **s775z** or **s775z-RGD** (10 nmol). (d) Plot of Tumor-to-Background Ratio (TBR) in living mice at different post-injection time points. (e) Plot of MPI for excised tumors normalized to thigh muscle from the same mouse sacrificed at 3 hr post-injection. Average for each cohort (N=4) is indicated by a black line, with error bars indicating \pm SEM. Representative NIR fluorescence image of an excised tumor is shown above each cohort. * indicates $p < 0.05$, and ** $p < 0.01$.

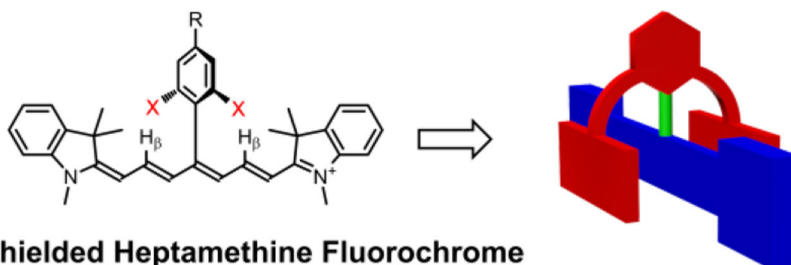


Scheme 1.
Chemical Structures of Heptamethine Cyanine Dyes.



Unshielded Heptamethine Fluorochrome

Rigid hydrophobic polyene core promotes: dye self-aggregation, interaction and reaction with other molecules.

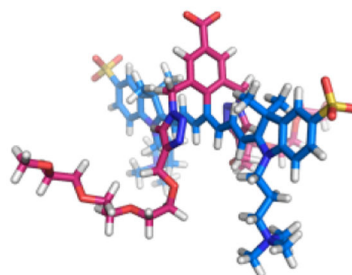


Shielded Heptamethine Fluorochrome

Central cyclohexyl ring is absent and the polyene is protected by two arms (X) directed over each face, which prevents: dye self-aggregation, interaction or reaction with other molecules.

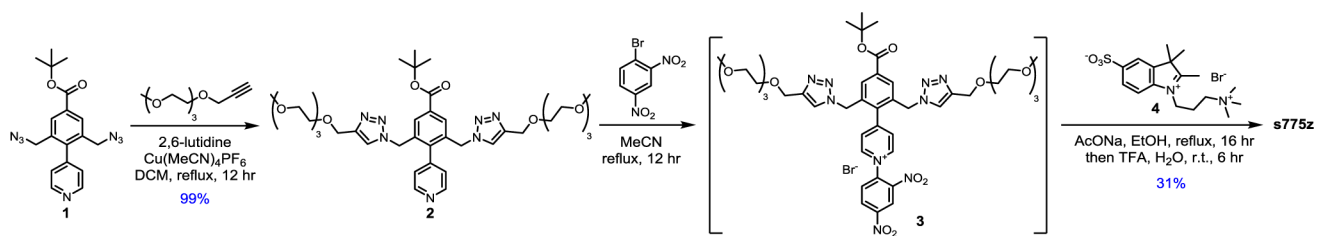
Molecular Model of s775z

The red-colored shielding arms, with triethyleneglycol chains, project over both faces of the polyene section of the blue-colored fluorochrome.



Scheme 2.

Basic Concept of a Sterically Shielded Heptamethine Cyanine Dye.



Scheme 3.
Synthesis of **s775z**.

Table 1.Spectral and Reactivity Properties of Dyes in PBS (pH 7.4).^[a]

	756z	s775z	UL766 ^[g]	ZW800-1 ^[g]	CW800 ^[g]
$\lambda_{\text{max}}^{\text{abs}}$ (nm)	681 (a) ^[f] 756 (m) ^[f]	775	766	770	775
$\lambda_{\text{max}}^{\text{em}}$ (nm)	773	794	789	788	796
ϵ (M ⁻¹ cm ⁻¹) (R ²) ^[b]	99,000 (0.942) ^[b]	201,000 (0.999)	229,000	246,000	242,000
QY ^[c]	0.097	0.090	0.095	0.135	0.090
Brightness ^[d]	9,600	18,000	22,000	33,000	22,000
Stable to nucleophiles ^[e]	Yes	Yes	Yes	No	No

^[a] Concentration range of dyes is 0 – 5 μM . All measurements were made at room temperature.

^[b] Molar absorptivity of monomer band, nonlinear relationship with concentration due to dye self-aggregation.

^[c] Quantum yield relative to **UL766**, error is $\pm 10\%$.

^[d] $\epsilon \times \text{QY}$, error is $\pm 15\%$.

^[e] Meso linkage is not cleaved by biological amines or thiols.^[10,12]

^[f] a = aggregate; m = monomer.

^[g] Spectral data from reference.^[10,23]